Title
Comparing Experimentally-Measured Sand's Times with Concentrated Solution Theory Predictions in a Polymer Electrolyte

Journal
Journal of The Electrochemical Society, 170(12)

ISSN
0013-4651

Authors
Hoffman, Zach J
Mistry, Aashutosh
Srinivasan, Venkat
et al.

Publication Date
2023-12-01

DOI
10.1149/1945-7111/ad1470

OPEN ACCESS

Comparing Experimentally-Measured Sand's Times with Concentrated Solution Theory Predictions in a Polymer Electrolyte

To cite this article: Zach J. Hoffman *et al* 2023 *J. Electrochem. Soc.* **170** 120524

Journal of The Electrochemical Society, 2023 **170** 120524

Comparing Experimentally-Measured Sand's Times with Concentrated Solution Theory Predictions in a Polymer Electrolyte

Zach J. Hoffman,[1,2,3] Aashutosh Mistry,[4,5] Venkat Srinivasan,[4,5,6] and Nitash P. Balsara[1,2,3,7,z]

[1]*Department of Chemical and Biomolecular Engineering, University of California, Berkeley, Berkeley, California 94720, United States of America*
[2]*Materials Sciences Division, Lawrence Berkeley National Laboratory, Berkeley, California 94720, United States of America*
[3]*Joint Center for Energy Storage Research (JCESR), Lawrence Berkeley National Laboratory, Berkeley, California 94720, United States of America*
[4]*Chemical Sciences and Engineering Division, Argonne National Laboratory, Lemont, Illinois 60439, United States of America*
[5]*Joint Center for Energy Storage Research, Argonne National Laboratory, Lemont, Illinois 60439, United States of America*
[6]*Argonne Collaborative Center for Energy Storage Science, Argonne National Laboratory, Lemont, Illinois 60439, United States of America*
[7]*Energy Storage and Distributed Resources Division, Lawrence Berkeley National Laboratory, Berkeley, CA 94720, United States of America*

We compare the electrochemically measured Sand's time, the time required for the cell potential to diverge when the applied current density exceeds the limiting current, with theoretical predictions for a 0.47 M poly(ethylene oxide) (5 kg mol^{-1})/LiTFSI electrolyte. The theoretical predictions are made using concentrated solution theory which accounts for both concentration polarization and polymer motion, using independently measured parameters that depend on concentration, c: conductivity (κ), salt diffusion coefficient (D), cationic transference number with respect to the solvent velocity (t_+^0), thermodynamic factor $\left(1+\frac{d\ln f_\pm}{d\ln c}\right)$, and partial molar volume of the salt ($\bar{V}$); $f_\pm$ is the mean molar activity coefficient of the salt. We find quantitative agreement between experimental data and theoretical predictions. We derive a generalized analytical expression for Sand's time for electrolytes based on dilute solution theory. This expression correctly predicts the divergence of the Sand's time at the limiting current, in agreement with experimental data and concentrated solution theory predictions. When the applied current is large compared to the limiting current, the analytical expression approaches the standard expression for Sand's time used in the literature.

 [DOI: 10.1149/1945-7111/ad1470]

Manuscript submitted June 27, 2023; revised manuscript received November 9, 2023. Published December 20, 2023.

List of Symbols

Symbol	Description
D	Salt diffusion coefficient (cm^2/s)
t_+^0	Cationic transference number with respect to the solvent velocity
$1+\frac{d\ln f_\pm}{d\ln c}$	Thermodynamic factor
$f_\pm$	Activity coefficient
c	Salt concentration (mole/liter)
c_0	Solvent concentration (mole/liter)
R_i	Interfacial resistance (Ohms)
A	Interfacial area (cm^2)
z_+	Charge number of cation
R	Gas constant (J/mol K)
T	Temperature (K)
F	Faraday's constant (C/mol)
L	Electrolyte thickness (μm)
t_{Sand}	Sand's time (min)
i	Current density (mA/cm^2)
i_L	Limiting current density (mA/cm^2)
V	Measured voltage (volts)
r	Molar ratio of lithium ions to ethylene oxide units ($r = [Li^+]/[EO]$)
$\bar{V}$	Partial molar volume (cm^3/mol)
κ	Ionic conductivity (S/cm)
ϕ	Electric potential corrected for interfacial effects (volts)
ν	Total number of ions
ν_+	Number of cations produced from salt dissociation
ν_-	Number of anions produced from salt dissociation
ρ_+	Current fraction

As current passes through a battery, salt concentration gradients develop within the electrolyte.[1] These gradients affect overall battery performance and can lead to cell failure. Understanding these salt concentration gradients is essential for identifying suitable electrolytes for various battery applications. Newman's concentrated solution theory provides a framework for predicting concentration gradients within an electrolyte.[2,3] For binary electrolytes, comprising of a salt that dissociates into cations and anions, and a solvent (which can either be a low molecular weight compound or a polymer), predicting concentration gradients requires knowledge of three transport parameters: conductivity (κ), salt diffusion coefficient (D), and cationic transference number with respect to the solvent velocity (t_+^0), along with two thermodynamic properties: thermodynamic factor $\left(1+\frac{d\ln f_\pm}{d\ln c}\right)$, where c is the molar salt concentration and $f_\pm$ is the salt activity coefficient, and molar volume of the salt ($\bar{V}$).[2–5] The experiments required to determine these parameters are challenging. It is perhaps not surprising that full electrochemical characterization, wherein the concentration dependence of all five parameters has been determined, is limited to relatively few electrolytes.[3,6–17]

The experiments required for full electrochemical characterization utilize small applied current densities (in the range of μA/cm^2). While the results of these measurements give values for the relevant transport and thermodynamic parameters, experiments at higher

[z]E-mail: nbalsara@berkeley.edu

current densities are necessary to probe the electrolyte performance at conditions relevant for battery applications. At sufficiently high current densities (in the range of mA/cm^2), the salt concentration in the vicinity of the negative electrode can reach zero. The current density at which this condition is obtained is called the limiting current density of the electrolyte.[5,10,18–21] If the thermodynamic and transport properties of an electrolyte are independent of concentration, then the limiting current density is given by

$$i_L = \frac{2FDc}{(1-\rho_+)L}, \quad [1]$$

where i_L is the limiting current density, F is Faraday's constant, ρ_+ is the current fraction, defined as the ratio of the final to initial current when the electrolyte is polarized in a symmetric cell, and L is the electrolyte thickness.[2] The importance of ρ_+ was established by Bruce and Vincent who showed that $\rho_+ = t_+^0$ in the limit of infinite dilution.[22] In this work, our efforts are focused on characterizing electrolytes at current densities above the limiting current density. In this regime, the measured electric potential diverges at a time that is referred to as Sand's time.[23–25] This is the time required for the salt concentration at the negative electrode to approach zero. In early work, Sand and coworkers showed that this time was related to both the salt diffusion coefficient and the transference number.[25] If the thermodynamic and transport properties of an electrolyte are independent of concentration, then Sand's time is given by

$$t_{Sand} = \pi D\left(\frac{Fc}{2i(1-\rho_+)}\right)^2, \quad [2]$$

where i is an applied current density above i_L.[25–27]

In this paper, we present data from measurements of Sand's time in a mixture of poly(ethylene oxide) (PEO), with number average molecular weight of 5 kg mol^{-1}, and lithium bis(trifluoromethanesulfonyl)imide (LiTFSI). The transport and thermodynamic parameters for this electrolyte have been reported in Refs. 7, 28, and 29 and can be found in Appendix A. This enables explicit calculation of Sand's time with no adjustable parameters. In a noteworthy publication, Lee et al. measured the Sand's time in a PEO/LiTFSI electrolyte (4,000 kg mol^{-1}) and interpreted their data in terms of a simplified theory.[30] In their theory, the transport and thermodynamic properties were treated as constants (some were adjusted and some were not), and the motion of the solvent molecules was ignored.[30] It is however well established that an applied electric field results in the motion of solvent molecules (PEO in our case) which in turn affects the motion of ions.[31–33] Rigorous solution of the relevant transport equations required determining both solvent velocity and concentration as a function of space and time. The analysis presented below is the first to include the effect of solvent motion and the concentration-dependence of the transport and thermodynamic properties of the electrolyte on Sand's time. We compare predictions and experimental data with no adjustable parameters. We find that Eq. 2 does not accurately describe the dependence of our predictions and measured t_{Sand} on i, as this equation is based on assumptions that are only valid at $i \gg i_L$. A universal expression for the dependence of t_{Sand} on i is derived using dilute solution theory, which agrees with the observed linear dependence of t_{Sand} on i. In the limit, at $i \gg i_L$, this expression reduces to Eq. 2.

Methods

Electrolyte preparation.—Poly(ethylene oxide) (PEO) with a molecular weight of 5 kg mol^{-1} (Polymer Source) was dried under active evacuation for 2 d at 90 °C. Lithium bis(trifluoromethanesulfonyl)imide (LiTFSI) (Sigma Aldrich) was dried under active evacuation for three days at 120 °C. Predetermined amounts of PEO and LiTFSI were combined and mixed in anhydrous tetrahydrofuran (THF) (Sigma Aldrich) in a capped vial at 60 °C under active stirring until fully dissolved. The cap was then removed, and the THF evaporated off. The electrolytes were then dried at 90 °C under active evacuation overnight to remove any remaining solvent. Preparation of electrolytes was performed in an argon-filled glovebox with water and oxygen levels below 2 ppm. The electrolytes used in this study all have the same salt concentration, r, the ratio of lithium ions to ethylene oxide moieties ($r = [Li^+]/[EO]$). The r value chosen was $r = 0.02$, or 0.47 M.

Lithium symmetric cells and Sand's time measurements.—Lithium symmetric cells were constructed inside an argon-filled glovebox with water and oxygen levels below 1 PPM. Lithium electrodes were prepared using lithium foil (MTI Corp.) that was first brushed then pressed with a mechanical press. The thickness of these electrodes was measured using a micrometer. Next silicone spacer material (VWR) of thicknesses 250 and 500 μm and an inner diameter of 3.175 mm, was filled with PEO/LiTFSI electrolyte. The lithium electrodes were pressed on each side of the electrolyte and the total thickness of the stack was measured, and the thickness of the electrolyte was calculated by subtracting the electrode thicknesses from the total stack thickness. Nickel tabs were attached on each side of the stack, and the cell was sealed in laminated pouch material.

Before electrochemical experiments were conducted, the cells were annealed on a custom heating stage at 90 °C for three hours. All electrochemical experiments were performed at 90 °C using a VMP3 Biologic potentiostat. Cells were first preconditioned by applying a current density of 0.02 mA cm^{-2} for 3 h then allowing the cells to relax at open circuit voltage (OCV) for 3 h, followed by impedance measurements. The same current density was then applied in the opposite direction followed by another period of relaxation and an impedance measurement. This process was performed for 5 cycles to form a stable solid electrolyte interface, which was determined by observing the interfacial resistance of each cell and ensuring it reached a constant value after multiple cycles. The resistance of the cell was measured using electrochemical impedance spectroscopy (EIS) with a frequency range of 1 MHz to 100 mHZ, and a sinus amplitude of 40 mV.

Sand's time measurements were performed by first taking an impedance measurement, then polarizing the cell with an applied current density, followed by an OCV step, and ending with an impedance measurement. Each cell was polarized with length-normalized current densities, iL, of 0.0075, 0.010, 0.0125, 0.015, 0.0175, and 0.020 mA cm^{-1}.

Modeling.—We use Newman's concentrated solution theory to theoretically understand concentration and potential evolution in a 0.47 M PEO(5 kg mol^{-1})/LiTFSI electrolyte when polarized at different current densities.[2,32,34] The concentration dependence of the relevant thermodynamic and transport properties have been previously measured for this electrolyte (Table A·I) and their continuous concentration-dependent functions (as plotted in Fig. 2 of Ref. 32) are used for the theoretical calculations.[7,28,29,35] The governing equations describing the evolution of ionic concentration are:

$$\frac{\partial c}{\partial t} = \frac{\partial}{\partial x}\left(D\left(1 - \frac{\mathrm{d}\ln c_0}{\mathrm{d}\ln c}\right)\frac{\partial c}{\partial x}\right) - \frac{i}{F}\frac{\partial c}{\partial x} - \frac{\partial}{\partial x}(cv_0), \quad [3]$$

$$\frac{\partial v_0}{\partial x} = \bar{V}\left\{\frac{\partial}{\partial x}\left(D\left(1 - \frac{\mathrm{d}\ln c_0}{\mathrm{d}\ln c}\right)\frac{\partial c}{\partial x}\right) - \frac{i}{F}\frac{\partial c}{\partial x}\right\}. \quad [4]$$

Note that x represents a moving interface attached to the left lithium-electrolyte interface which strips when the ionic current flows in the $+x$ direction. The velocity of this moving interface is linked to the

applied current density, i, and constant when the Li-electrolyte-Li cell is polarized at constant current densities. Based on the $c(x,t)$ profile obtained by solving the aforementioned equations, the electrolyte potential, $\Delta\phi$, can be computed using concentration-dependent conductivity, κ, cationic transference number, t_+^0, and thermodynamic factor, $\left(1 + \frac{\mathrm{d}\ln f_\pm}{\mathrm{d}\ln c}\right)$, as per the following expression:

$$\Delta\phi = \phi_{x=0} - \phi_{x=L} = i\int_L^0 \frac{1}{\kappa}\mathrm{d}x$$

$$+ \frac{2RT}{F}\int_{c_{x=L}}^{c_{x=0}} (1 - t_+^0)\left(1 + \frac{\mathrm{d}\ln f_\pm}{\mathrm{d}\ln c}\right)\mathrm{d}\ln c. \quad [5]$$

Notice that the first term on the right is the ohmic drop, i.e., related to finite ionic conductivity of the electrolyte, and the second term represents the overpotential related to the concentration polarization across the electrolyte thickness.

$$\Delta\phi_{\text{ohmic}} = i\int_L^0 \frac{1}{\kappa}\mathrm{d}x, \quad [6]$$

$$\Delta\phi_{\text{concentration}}$$

$$= \frac{2RT}{F}\int_L^0 (1 - t_+^0)\left(1 + \frac{\mathrm{d}\ln f_\pm}{\mathrm{d}\ln c}\right)\mathrm{d}\ln c. \quad [7]$$

These expressions are numerically solved using the Finite Volume Method (details are provided in Ref. 32). The current density, i, at which the electrolyte is polarized explicitly appears in these equations and additionally in the concentration boundary conditions at both lithium-electrolyte interfaces:

$$-D\left(1 - \frac{\mathrm{d}\ln c_0}{\mathrm{d}\ln c}\right) = (1 - t_+^0)\frac{i}{F}. \quad [8]$$

We have assumed that the reaction overpotentials are negligible compared to the bulk overpotentials across the thick electrolytes examined herein.

Results and Discussion

Sand's time measurements are made by applying a constant current density to a Li-electrolyte-Li cell and measuring the resulting electric potential. The experimentally measured potential includes the potential drop across the solid electrolyte interphase (SEI). Since we are only interested in the potential drop across the electrolyte, this contribution is subtracted. The potential of interest is defined as

$$\Delta\phi(t) = V(t) - R_i iA, \quad [9]$$

where V is the measured voltage, R_i is the interfacial resistance, and A is the interfacial area. The resistance used for these calculations is the interfacial resistance measured by ac impedance after polarization. The interfacial resistance of our electrolytes was typically an order of magnitude smaller than the bulk resistance.

In Fig. 1, we show $\Delta\phi$ as a function of time, t, at various values of iL, the length normalized current density. We prefer iL to i to account for the fact that the electrolyte thickness in each of our cells is not identical, and the characteristics of our symmetric cells are governed by the product, iL. Figure 1a shows characteristic data collected from our electrochemical experiments, for a cell with an electrolyte thickness of 576 μm. At each value of iL the electric potential increases gradually at early times. Beyond a characteristic time that decreases with increasing current density, the potential rapidly approaches the cutoff potential of 1.5 V.

Equations 3–8 were solved using parameters for our PEO/LiTFSI electrolyte. These parameters are given in Table A·I. Figure 1b shows the calculated potential as a function of time modeled for a salt concentration of 0.47 M and a thickness $L = 500$ μm.[32] The current density used in the calculations were chosen to match the iL used for the experimental measurements. At $iL \leqslant 0.01$ mA cm^{-1}, the correspondence between theory and experiment is nearly quantitative. At the smallest applied current density, experiments show a divergence of cell potential while theory does not. This discrepancy is well within the uncertainty of the transport and thermodynamic parameters. The gray lines in Figs. 1a and 1b were used to determine Sand's time. These lines reflect the time at which the cell potential diverges in both theory and experiment.

Figure 2a shows the time dependence of $\Delta\phi$ for a typical calculation ($iL = 0.015$ mA cm^{-1}, $L = 500$ μm). The electric potential contains two contributions: $\Delta\phi = \Delta\phi_{ohmic} + \Delta\phi_{concentration.}$ $\Delta\phi_{ohmic}$ is the component of the potential due to the resistance of the electrolyte, which is related to κ by Ohm's law. Equation 6 can be written as

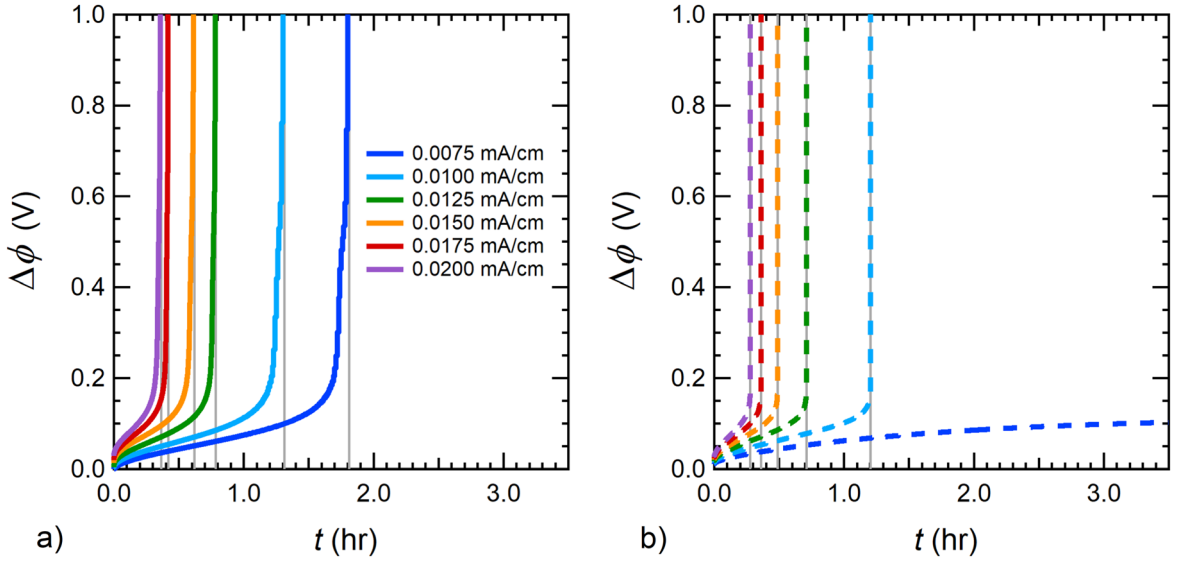

Figure 1. Electric potential, $\Delta\phi$, plotted as a function of time, t, in response to length normalized current densities, iL. (a) Measured data from a 0.47 M PEO/LiTFSI electrolyte with a thickness, L, of 576 μm and (b) predicted using concentrated solution theory for a 0.47 M PEO/LiTFSI electrolyte with $L = 500$ μm. The colors of the curves in (b) correspond with the same values of iL listed in (a). Gray lines indicate the time at which the potential diverged each value of iL for experiments and theory. All experimental measurements were made at 90 °C, and predictions utilize PEO/LiTFSI properties measured at 90 °C (Table A·I).

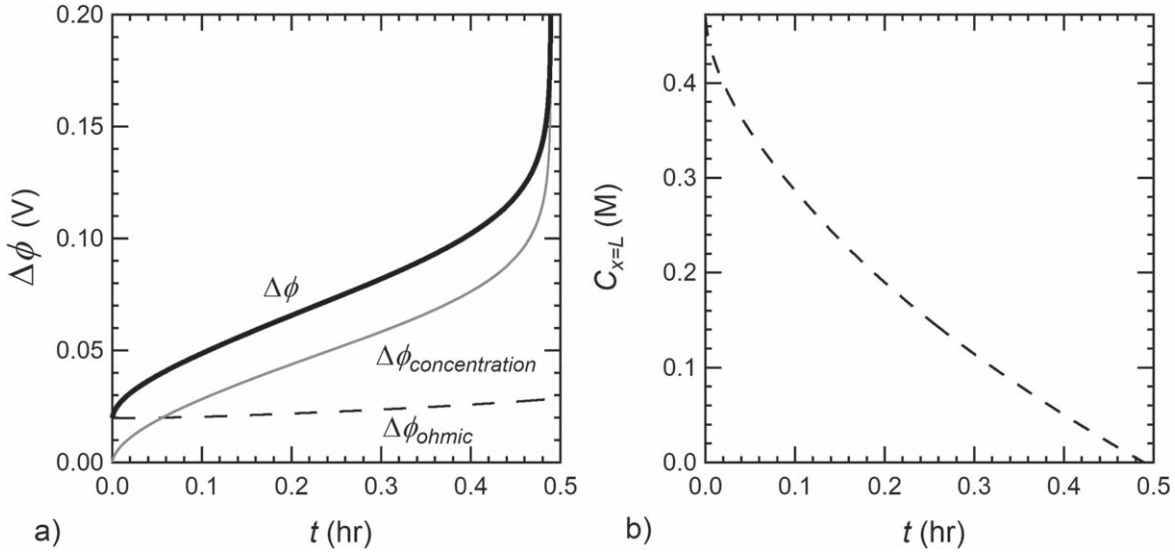

Figure 2. (a) Predicted electric potential (solid black line), $\Delta\phi$, and the components of the potential due to ohmic effects (dashed black line), $\Delta\phi_{ohmic}$, and concentration polarization (solid gray line), $\Delta\phi_{concentration}$, as functions of time, t. (b) Predicted lithium salt concentration at the negative electrode, $c_{x=L}$, versus t. These predictions are for a 0.47 M PEO/LiTFSI electrolyte, $L = 500$ μm, polarized at $iL = 0.015$ mA cm^{-1}. Predictions utilize PEO/LiTFSI properties measured at 90 °C (Table A·I).

$$\Delta\phi_{ohmic} = i\frac{L}{\kappa_{avg}}. \quad [10]$$

As the cell is polarized, the concentration varies across the cell, and κ_{avg} reflects the average conductivity of the electrolyte. $\Delta\phi_{concentration}$ is obtained by subtracting $\Delta\phi_{ohmic}$ from $\Delta\phi$. In Fig. 2a, $\Delta\phi$ (solid black line), $\Delta\phi_{ohmic}$ (dashed black line), and $\Delta\phi_{concentration}$ (solid gray line) are plotted as a function of time. At $t = 0^+$, $\Delta\phi = \Delta\phi_{ohmic}$. Salt concentration gradients grow with increasing time, but this has a minimal effect on $\Delta\phi_{ohmic}$. At $t = 0^+$, $\Delta\phi_{concentration}$ is zero. However, the growth of salt concentration gradients is reflected in the increase in $\phi_{concentration}$. Figure 2b shows the salt concentration at the negative electrode, $c_{x=L}$, as a function of time. As $c_{x=L}$ smoothly approaches a value close to zero at $t = 0.5$ h, $\Delta\phi_{concentration}$diverges. This connection between potential divergence and concentration was first recognized by Sand.[25]

Sand's time depends on two parameters, the applied current density, i, and electrolyte thickness, L. Rearranging Eq. 2 gives

$$\frac{t_{Sand}}{L^2} = \pi D\left(\frac{Fc}{2(iL)(1-\rho_+)}\right)^2, \quad [11]$$

which shows that it is convenient to consider the dependence of the Sand's time on the length normalized current density, iL, and L. We use the model to predict the effect of L on t_{Sand} at $iL = 0.010$ mA cm^{-1}. These results are shown in Fig. 3a. As expected, t_{Sand} increases with increasing L. At $L = 100$ μm t_{Sand} is 0.3 h, while at $L = 1000$ μm $t_{Sand} = 4.7$ h. In Fig. 1a we reported the Sand's time at $iL = 0.01$ mA cm^{-1} for $L = 576$ μm. We repeated this experiment for three

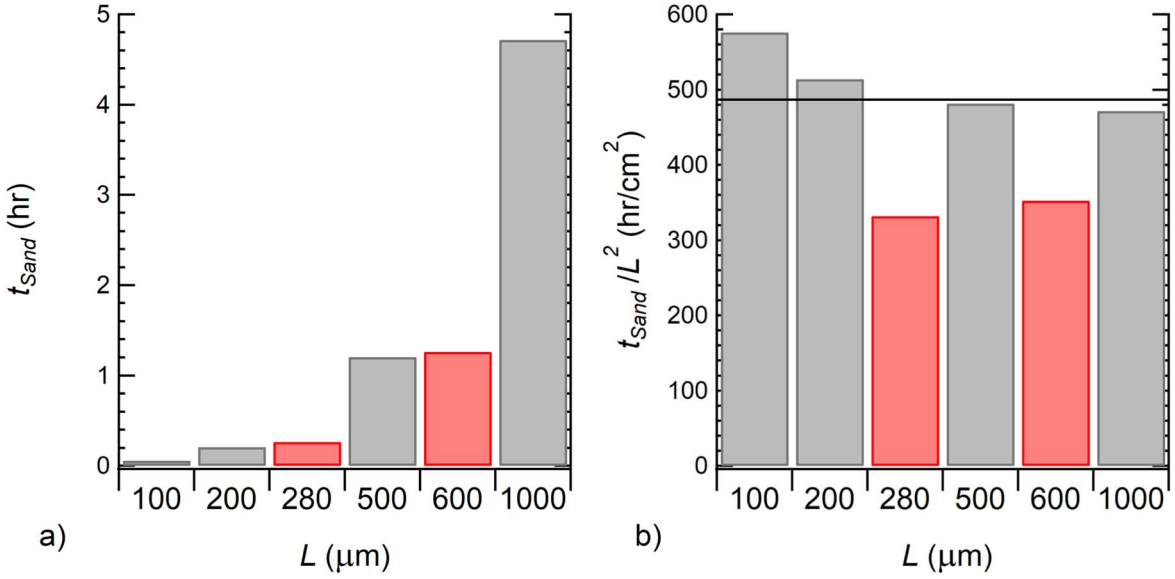

Figure 3. (a) Sand's times, t_{Sand}, plotted for various 0.47 M PEO/LiTFSI electrolyte thicknesses in response to polarization at $iL = 0.010$ mA cm^{-1}. (b) Length normalized Sand's times, t_{Sand}/L^2, plotted for various 0.47 M PEO/LiTFSI electrolyte thicknesses. The black line indicates the value of t_{Sand}/L^2 predicted from Eq. 11. Gray bars indicate predictions from concentrated solution theory, and red bars indicate the average Sand's time from experimental measurements. All experimental measurements were made at 90 °C, and predictions utilize PEO/LiTFSI properties measured at 90 °C (Table A·I).

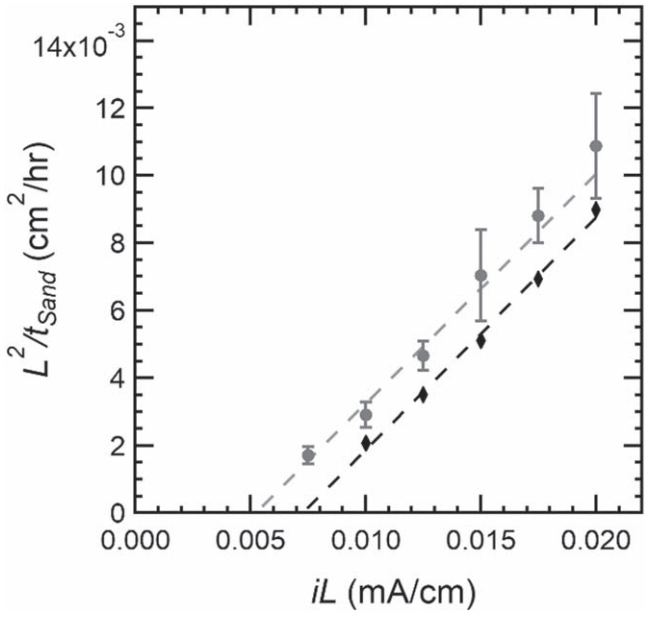

Figure 4. Length normalized inverse Sand's time, L^2/t_{Sand}, plotted as a function of length normalized current density, iL. The data is reported from experimental cells with nominal thicknesses of 280 μm and 600 μm where the gray circles represent the average value of L^2/t_{Sand} and the error bars represent the standard deviation and predictions from concentrated solution theory for a cell with a thickness of 500 μm (black rhombuses). The gray dashed line is a linear fit of the experimental data, and the black dashed line is a linear fit of predicted Sand's time. All experimental measurements were made at 90 °C, and predictions utilize PEO/LiTFSI properties measured at 90 °C (Table A·I).

independent cells with an average value of $L = 600$ μm. In addition, we studied two cells with an average value of $L = 280$ μm with the same value of iL (0.01 mA cm^{-1}). The experimental results are also shown in Fig. 3a. The experiments and theoretical predictions are in quantitative agreement (within the uncertainty of the transport and thermodynamic parameters used in the calculations).

Figure 3b shows the same results but plotted in the format suggested by Eq. 11. Here we show t_{Sand}/L^2 as a function of L for a fixed $iL = 0.01$ mA cm^{-1}. Also shown in Fig. 3b is the value from Eq. 11, with parameters for our 0.47 M PEO/LiTFSI electrolyte ($D = 7.8 \times 10^{-8}$ cm^2/s, $\rho_+ = 0.15$). Calculations based on concentrated solution theory approach Eq. 11 as L is increased from 100 to 1000 μm. The value of t_{Sand}/L^2 from Eq. 11 is 484 h/cm^2. The experimental data obtained at two different thicknesses are reasonably consistent with theoretical predictions.

The Sand's time experiments were conducted at different values of iL. Figure 4 shows these results on a plot of L^2/t_{Sand} versus iL for electrolyte thicknesses in the vicinity of 280 and 600 μm where the gray circles represent the average value of L^2/t_{Sand} and the error bars represent the standard deviation. Also shown in this figure are theoretical calculations for $L = 500$ μm (black rhombuses). Note that the theoretically predicted $L^2/t_{Sand}$is a weak function of L. We see that L^2/t_{Sand} is a linear function of iL. By fitting the data in Fig. 4. to a line, we can identify the value of iL at which L^2/t_{Sand} approaches zero, or $iL \to i_L L$. In other words, the limiting current density is the current density at which the Sand's time approaches infinity. The slope and intercept of a linear fit of the experimental data are 0.678 and -3.53×10^{-3} respectively and 0.689 and -5.01×10^{-3} for concentrated solution theory predictions. This calculation results in $i_L L$ values of 0.0052 ± 0.001 mA cm^{-1} for the experimental data and 0.0073 ± 0.0007 mA cm^{-1} for the theoretical predictions. The error of our calculations is determined through propagation of error of the coefficients from our linear fits. It is challenging to directly measure i_L in 5 kg mol^{-1} PEO/LiTFSI electrolytes, as the low molecular weight provides little resistance to the growth of dendrites.[36–40] The large polarization times required for limiting current density measurements correspond with high cell failure rates.[18–21,41,42] The methodology based on Sand's time provides a convenient approach for measuring limiting current as it uses much shorter polarization times which are less likely to be affected by dendrite growth.

The standard equation for analyzing Sand's time data, Eq. 2, is inconsistent with both the theoretical calculations and experimental data presented in Fig. 4. It can readily be seen that Eq. 2 predicts that $t_{Sand} \to \infty$ as $i \to 0$, while our model predicts that that $t_{Sand} \to \infty$ as $i \to i_L$. This discrepancy arises because of the simplifying assumptions made to arrive at Eq. 2. In particular, this equation is based on the simplifying assumptions that (1) the transport parameters are independent of concentration, and (2) $i \gg i_L$ and in this limit, the concentration gradients are restricted to narrow regions near the electrode. In this limit, the electrolyte concentration in the center of the cell is uniform as depicted in Fig. 5a. However, as i approaches i_L, the second simplification is not valid and the concentration gradients are nonnegligible throughout the cell (Fig. 5a). In Appendix C, we derive a general expression for the Sand's time for an electrolyte with concentration-independent transport properties that is valid as i approaches i_L and in the limit, $i \gg i_L$. The general dependence of t_{Sand} on i is given by:

$$1 = 8\left(\frac{i}{i_L}\right)\sum_{n=1}^{\infty}\frac{1}{\beta_n^2}\left(1 - e^{-\beta_n^2\left(\frac{Dt_{\text{Sand}}}{L^2}\right)}\right). \qquad [12]$$

where $\beta_n = (2n - 1)\pi$ is the Eigen value. Equation 12 is a nonlinear equation that can be solved for t_{Sand} if i/i_L, D and L are known. The solution to Eq. 12 can be represented by a single curve if i/i_L is plotted versus $L^2/(Dt_{Sand})$. This is shown in Fig. 5c. Equation 2 can be rewritten as

$$\frac{Dt_{Sand}}{L^2} = \frac{\pi}{16}\left(\frac{i_L}{i}\right)^2, \qquad [13]$$

and this equation is also shown in Fig. 5b. In the regime $i/i_L > 1.5$, Eqs. 12 and 13 are indistinguishable, $t_{Sand} \propto i^{-2}$. At lower current densities, however, there are significant differences between the two equations. In particular, Eq. 13 gives nonzero values for t_{Sand} in the regime $i/i_L < 1$ which are unphysical. In contrast, Eq. 12 predicts that t_{Sand} is a linear function of i^{-1}, and $t_{Sand} \to \infty$ as $i \to i_L$.

In Fig. 5c, we compare the predictions of Eq. 12 with both experiments and the full simulations. Equation 12 is shown as a continuous curve (using $c = 0.47$M properties $D = 7.8 \times 10^{-8}$ cm^2/s and $\rho_+ = 0.15$). The quantitative difference between the detailed simulations and the analytical trends are due to the concentration-dependent electrolyte properties and the concentrated solution theory description of electrolyte transport in the detailed simulations.

Conclusions

We present an approach for calculating Sand's time in electrolytes using concentrated solution theory. The theory is rigorous and accounts for both concentration polarization and motion of all three species, the cation, the anion, and the solvent (a polymer in our case). Using this theory requires the knowledge of three transport parameters: κ, D, t_+^0, and two thermodynamic parameters: $1 + \frac{d\ln f_\pm}{d\ln c}$ and $\bar{V}$. All five parameters depend on concentration. We present a limited test of the theory using experimentally determined Sand's time of a 0.47 M PEO(5 kg mol^{-1})/LiTFSI electrolyte. We examine the effects of both current density and electrolyte thickness on Sand's time. The experimental data are in excellent agreement with the rigorous theoretical calculations. This agreement is obtained without resorting to any adjustable parameters. We derive an analytical expression for t_{Sand} that is valid if the transport parameters are independent of concentration, regardless of the ratio i/i_L. The rigorous calculations are

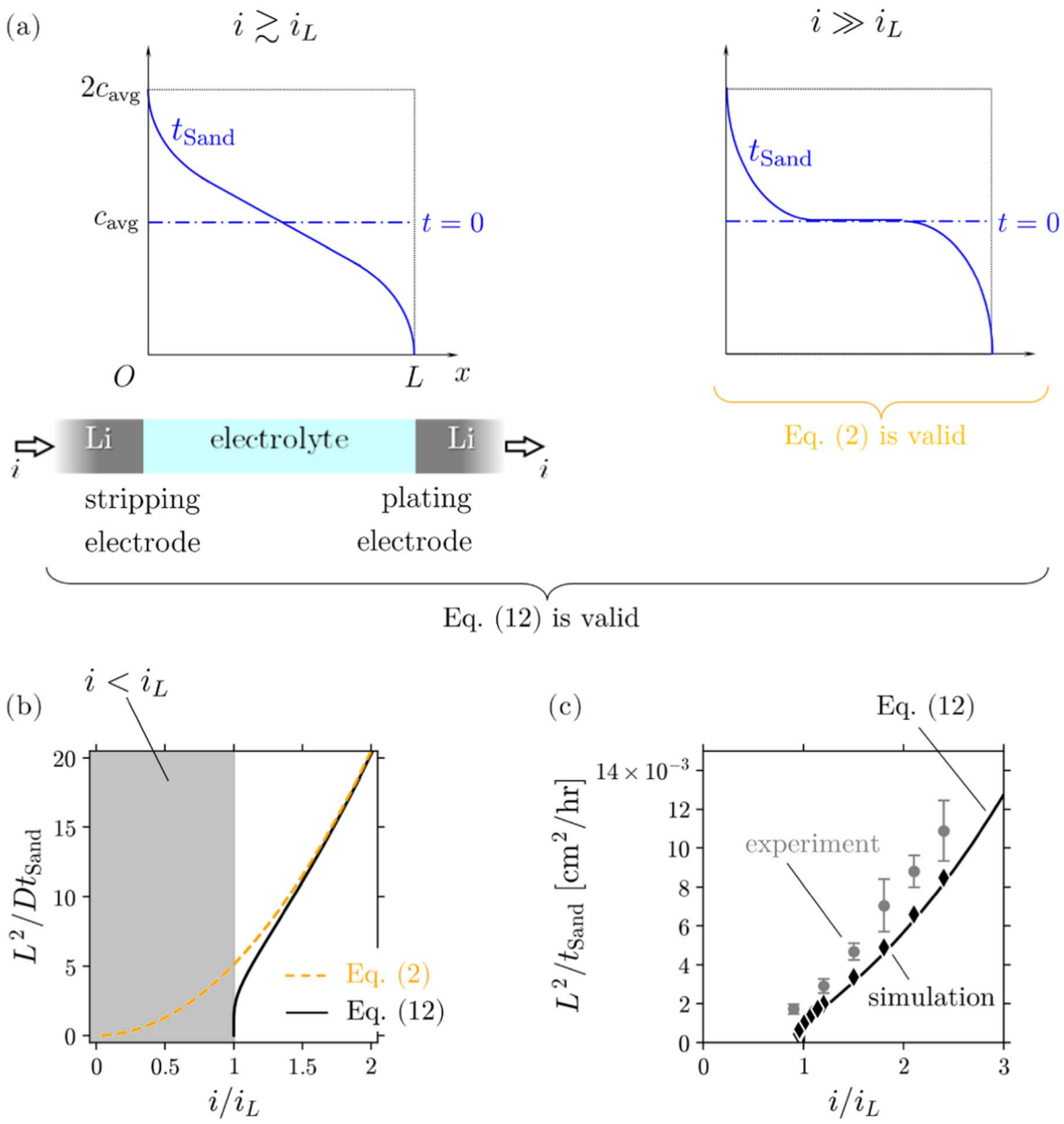

Figure 5. (a) A schematic diagram representing different regimes of electrolyte polarization at varying current densities, i, relative to the limiting current density, i_L. In the limit of very large currents, i.e., $i \gg i_L$, the salt concentration gradients are close to the two electrodes and Eq. 13 is valid if the transport properties are concentration independent. When i is comparable to i_L, the concentration gradients are finite throughout the cell and the more general Eq. 12 is applicable. (b) presents the analytical solutions for Sand's time, t_{Sand}, in the two current density regimes: $i \gg i_L$ (Eq. 13) and $i \gtrsim i_L$ (Eq. 12). (c) presents Eq. 12 with the full simulation (diamonds) and experimental data (circles). L is the electrolyte thickness and D is the diffusion coefficient.

in reasonable agreement with the analytical expression. The electrolyte examined in this work is sufficiently dilute, and results obtained using the rigorous theory are not very different from simplified models based on dilute solution theory. In the future, we plan to test the theory using experiments on more concentrated electrolytes. These experiments are challenging due to the formation of lithium dendrites at currents exceeding the limiting current. Efforts to resolve these challenges are currently underway.

Acknowledgments

This work was intellectually led by the Joint Center for Energy Storage Research (JCESR), an Energy Innovation Hub funded by the U.S. Department of Energy, Office of Science, Office of Basic Energy Science, under Contract No. DE-AC02–06CH11357, which supported work conducted by Z. J. H. under the supervision of N.P. B.A.M. and V.S. acknowledge the support by UChicago Argonne, LLC, Operator of Argonne National Laboratory ("Argonne"). Argonne, a U.S. Department of Energy Office of Science laboratory, is operated under Contract No. DE-AC02–06CH11357. The U.S. Government retains for itself, and others acting on its behalf, a paid-up nonexclusive, irrevocable worldwide license in said article to reproduce, prepare derivative works, distribute copies to the public, and perform publicly and display publicly, by or on behalf of the Government. The Department of Energy will provide public access to these results of federally sponsored research in accordance with the DOE Public Access Plan: http://energy.gov/downloads/doe-public-access-plan.

Appendix A

A.1. PEO/LiTFSI properties

Table A·I. Properties of PEO/LiTFSI electrolytes at 90 °C, taken from Refs. 7, 28, and 29.

c (M)	ρ (g/cm^3)	t_+^0	κ (S/cm)	D (cm^2/s)	$1+\frac{d\ln f_\pm}{d\ln c}$	ρ_+
0.25	1.160	0.07	2.7×10^{-4}	6.0×10^{-8}	0.45	0.18
0.47	1.180	0.23	7.5×10^{-4}	7.8×10^{-8}	0.75	0.15
0.87	1.210	0.40	1.8×10^{-3}	1.0×10^{-7}	1.93	0.11
1.20	1.230	0.33	2.0×10^{-3}	1.3×10^{-7}	2.69	0.11
1.59	1.330	0.43	2.2×10^{-3}	1.1×10^{-7}	4.24	0.10
1.87	1.365	0.20	1.3×10^{-3}	8.4×10^{-8}	3.78	0.09
2.11	1.38	0.08	1.1×10^{-3}	7.0×10^{-8}	3.92	0.08
2.38	1.43	−0.08	9.9×10^{-4}	5.8×10^{-8}	3.93	0.07
2.58	1.45	−0.38	1.3×10^{-3}	9.4×10^{-8}	3.51	0.06
2.76	1.47	0.10	1.6×10^{-3}	9.0×10^{-8}	6.03	0.07
3.05	1.52	0.41	1.2×10^{-4}	6.5×10^{-8}	10.84	0.10
3.36	1.58	0.33	6.4×10^{-4}	6.3×10^{-8}	10.89	0.16
3.49	1.57	0.18	4.0×10^{-4}	5.9×10^{-8}	10.06	0.18

Appendix B

B.1. Literature derivation for Sand's time, $i \gg i_L$.—The electrodeposition literature uses Eq. 2 to prescribe the Sand time, t_{Sand}, to represent the time it takes for the concentration cations to drop to zero at the plating electrode. The corresponding governing equation to describe salt polarization,

$$\frac{\partial c}{\partial t} = D\frac{\partial^2 c}{\partial x^2}, \qquad [B\cdot1]$$

assumes that the electrolyte behaves as a dilute solution and its properties are constant (in contrast to the full set of concentrated solution theory governing equations, Eqs. 3–8). Equation B·1 is solved subject to the boundary conditions

$$-D\frac{\partial c}{\partial x}\bigg|_{x=0} = (1-\rho_+)\frac{i}{F}, \qquad [B\cdot2]$$

$$c(x\to\infty, t) = c_{avg}, \qquad [B\cdot3]$$

and initial condition

$$c(x, t=0) = c_{avg}. \qquad [B\cdot4]$$

Note that Eq. B·2 uses the dilute solution theory transference number, ρ_+. Equation B·3 implicitly assumes that the concentration gradients manifest over a short distance, $\delta \ll L/2$, such that the concentration in the center of the cell is fairly invariant and same as the initial concentration. Such an assumption can only be justified for current densities, i, much larger than the (dilute solution theory-based) limiting current densities, i_L, defined in Eq. 1.

Equations B·1 to B·4 can be alternatively expressed in terms of the concentration change, $c'(x, t)$, relative to the initial uniform concentration.

$$\frac{\partial c'}{\partial t} = D\frac{\partial^2 c'}{\partial x^2}, \qquad [B\cdot5]$$

subject to the boundary conditions

$$-D\frac{\partial c'}{\partial x}\bigg|_{x=0} = (1-\rho_+)\frac{i}{F}, \qquad [B\cdot6]$$

$$c'(x\to\infty, t) = 0, \qquad [B\cdot7]$$

and initial condition

$$c'(x, t=0) = 0. \qquad [B\cdot8]$$

Using the initial condition B·8, Eqs. B·5 to B·7 can be expressed in the Laplace s-domain as

$$\frac{d^2\mathbb{C}}{dx^2} = \lambda^2\mathbb{C}, \qquad [B\cdot9]$$

subject to the boundary conditions

$$-D\frac{d\mathbb{C}}{dx}\bigg|_{x=0} = (1-\rho_+)\frac{i}{Fs}, \qquad [B\cdot10]$$

$$\mathbb{C}(x\to\infty, t) = 0. \qquad [B\cdot11]$$

Here

$$\mathbb{C}(x, s) = \int_0^\infty e^{-st}c'(x, t)dt, \qquad [B\cdot12]$$

is the Laplace transformed concentration, and,

$$\lambda^2 = \frac{s}{D}. \qquad [B\cdot13]$$

Equation B·10 can be easily solved for $\mathbb{C}(x, s)$ to give

$$\mathbb{C}(x, s) = \frac{\lambda}{s^2}(1-\rho_+)\frac{i}{F}e^{-\lambda x}. \qquad [B\cdot14]$$

Using inverse Laplace transform tables, $\mathbb{C}(x, s)$ can be transformed back to the time domain:

$$c'(x, t) = \frac{1}{\sqrt{D}}(1-\rho_+)\frac{i}{F}\left\{2\sqrt{\frac{t}{\pi}}e^{-\frac{x^2}{4Dt}} - \frac{x}{\sqrt{D}}\text{erfc}\left(\frac{x}{2\sqrt{Dt}}\right)\right\}, \qquad [B\cdot15]$$

where erfc(x) is complementary error function in x. Equivalently, the spatiotemporal variation of the salt concentration is:

$$c(x, t) = c_{avg} + \frac{1}{\sqrt{D}}(1-\rho_+)\frac{i}{F}\left\{2\sqrt{\frac{t}{\pi}}e^{-\frac{x^2}{4Dt}} - \frac{x}{\sqrt{D}}\text{erfc}\left(\frac{x}{2\sqrt{Dt}}\right)\right\}. \qquad [B\cdot16]$$

As mentioned earlier, for $i \gg i_L$, the salt concentration on the plating electrode, i.e., $x = L$, drop to zero. Equivalently, the salt concentration on the stripping electrode, i.e., $x = 0$, reaches $2c_{avg}$. Accordingly, substituting $x = 0$ and $c(x = 0, t) = 2c_{avg}$, in Eq. B·16 gives

$$c_{\text{avg}} = \frac{1}{\sqrt{D}}(1-\rho_+)\frac{i}{F}2\sqrt{\frac{t_{\text{Sand}}}{\pi}}. \quad [\text{B}\cdot17]$$

Equation B·17 can be rearranged to show

$$t_{\text{Sand}} = \frac{\pi}{4}D\left(\frac{Fc_{\text{avg}}}{(1-\rho_+)i}\right)^2, \quad [\text{B}\cdot18]$$

which is identical to Eq. 2 used in the literature. Using the definition of the limiting current density based on dilute solution theory at constant properties, i.e., Eq. 1, Eq. B·18 can be reexpressed as

$$\frac{Dt_{\text{Sand}}}{L^2} = \frac{\pi}{16}\left(\frac{i_L}{i}\right)^2. \quad [\text{B}\cdot19]$$

Note that Dt_{Sand}/L^2 can be thought of a dimensionless Sand time.

Appendix C

C.1. Sand's time for any overlimiting current densities, $i \geqslant i_L$.—Given the boundary condition Eq. B·3, the Sand time expressions (Eqs. B·18 and B·19) are only valid for current densities much larger than the limiting values. This boundary condition can be replaced with

$$c\left(x=\frac{L}{2},\, t\right) = c_{\text{avg}}, \quad [\text{C}\cdot1]$$

to obtain a universally valid Sand time expression. Following similar steps as before, one can show that the solution of governing Eq. B·1 subject to boundary conditions B2 and C1 and initial condition B4 is

$$c(x,\, t) = c_{\text{avg}} + 8c_{\text{avg}}\left(\frac{i}{i_L}\right)\sum_{n=1}^{\infty}\frac{(-1)^n}{\beta_n^2}\sin\left(\beta_n\left(\frac{x}{L}-\frac{1}{2}\right)\right)\left(1-e^{-\beta_n^2\left(\frac{Dt}{L^2}\right)}\right), \quad [\text{C}\cdot2]$$

where $\beta_n = (2n-1)\pi$ is the Eigen value.

Same as before Eq. C·2 can be used to estimate the time, t_{Sand}, it takes for the salt concentration to reach $2c_{\text{avg}}$ at the stripping electrode (identical to the time it takes for the salt concentration to drop to zero at the plating electrode).

$$\therefore\ 1 = 8\left(\frac{i}{i_L}\right)\sum_{n=1}^{\infty}\frac{1}{\beta_n^2}\left(1-e^{-\beta_n^2\left(\frac{Dt_{\text{Sand}}}{L^2}\right)}\right). \quad [\text{C}\cdot3]$$

It can be shown that for $i \gg i_L$, Eq. C·3 collapses to Eq. B·19 as expected. Note that while Eq. B·19 explicitly expresses t_{Sand} in terms of electrolyte properties and operating conditions, Eq. C·3 is an implicit expression for t_{Sand} in terms of the same electrolyte properties and operating conditions. An additional complexity is Eq. C·3 is an infinite convergent sum.

ORCID

Zach J. Hoffman https://orcid.org/0000-0002-8989-8077
Aashutosh Mistry https://orcid.org/0000-0002-4359-4975
Nitash P. Balsara https://orcid.org/0000-0002-0106-5565

References

1. Y. Choo, D. M. Halat, I. Villaluenga, K. Timachova, and N. P. Balsara, *Prog. Polym. Sci.*, **103**, 101220 (2020).
2. J. Newman and K. E. Thomas-Alyea, *Electrochemical Systems* (John Wiley & Sons, Hoboken, New Jersey) 3rd ed. (2004).
3. Y. Ma, M. Doyle, T. F. Fuller, M. M. Doeff, L. C. De Jonghe, and J. Newman, *J. Electrochem. Soc.*, **142**, 1859 (1995).
4. L. Onsager, *Ann. N. Y. Acad. Sci.*, **46**, 241 (1945).
5. J. D. Bazak, J. P. Allen, S. A. Krachkovskiy, and G. R. Goward, *J. Electrochem. Soc.*, **167**, 140518 (2020).
6. Z. J. Hoffman, D. B. Shah, and N. P. Balsara, *Solid State Ionics*, **370**, 115751 (2021).
7. D. M. Pesko, K. Timachova, R. Bhattacharya, M. C. Smith, I. Villaluenga, J. Newman, and N. P. Balsara, *J. Electrochem. Soc.* (2017).
8. D. B. Shah, H. Q. Nguyen, L. S. Grundy, K. R. Olson, S. J. Mecham, J. M. Desimone, and N. P. Balsara, *Phys. Chem. Chem. Phys.* (2019).
9. J. Landesfeind and H. A. Gasteiger, *J. Electrochem. Soc.* (2019).
10. Y. Choo, R. L. Snyder, N. J. Shah, B. A. Abel, G. W. Coates, and N. P. Balsara, *J. Electrochem. Soc.*, **169**, 020538 (2022).
11. L. O. Valøen and J. N. Reimers, *J. Electrochem. Soc.* (2005).
12. H. Lundgren, M. Behm, and G. Lindbergh, *J. Electrochem. Soc.* (2015).
13. A. A. Wang, T. Hou, M. Karanjavala, and C. W. Monroe, *Electrochim. Acta*, **358**, 136688 (2020).
14. T. Hou and C. W. Monroe, *Electrochim. Acta*, **332**, 135085 (2020).
15. J. Landesfeind, T. Hosaka, M. Graf, K. Kubota, S. Komaba, and H. A. Gasteiger, *J. Electrochem. Soc.*, **168**, 040538 (2021).
16. A. Nyman, M. Behm, and G. Lindbergh, *Electrochim. Acta* (2008).
17. D. T. Hickson, D. M. Halat, A. S. Ho, J. A. Reimer, and N. P. Balsara, *Phys. Chem. Chem. Phys.*, **24**, 26591 (2022).
18. G. K. Sethi, L. Frenck, S. Sawhney, S. Chakraborty, I. Villaluenga, and N. P. Balsara, *Solid State Ionics*, **368**, 115702 (2021).
19. J. A. Maslyn, L. Frenck, V. D. Veeraraghavan, A. Müller, A. S. Ho, N. Marwaha, W. S. Loo, D. Y. Parkinson, A. M. Minor, and N. P. Balsara, *Macromolecules*, **54**, 4010 (2021).
20. L. Frenck, V. D. Veeraraghavan, J. A. Maslyn, and N. P. Balsara, *Electrochim. Acta*, 139911 (2022), https://linkinghub.elsevier.com/retrieve/pii/S0013468622000834.
21. D. A. Gribble, L. Frenck, D. B. Shah, J. A. Maslyn, W. S. Loo, K. I. S. Mongcopa, D. M. Pesko, and N. P. Balsara, *J. Electrochem. Soc.* (2019).
22. P. G. Bruce and C. A. Vincent, *J. Electroanal. Chem.* (1987).
23. A. Mistry and V. Srinivasan, *MRS Adv.*, **4**, 2843 (2019).
24. M. Rosso, T. Gobron, C. Brissot, J. N. Chazalviel, and S. Lascaud, *J. Power Sources*, **97–98**, 804 (2001).
25. H. S. Sand, *Proc. Phys. Soc. London*, **17**, 496 (1899).
26. D. Devaux, H. Leduc, P. Dumaz, M. Lecuyer, M. Deschamps, and R. Bouchet, *Front. Energy Res.*, **7**, 168 (2020).
27. L. Stolz, G. Homann, M. Winter, and J. Kasnatscheew, *Mater. Today*, **44**, 9 (2021).
28. H.-K. Kim, N. P. Balsara, and V. Srinivasan, *J. Electrochem. Soc.*, **167**, 110559 (2020).
29. D. M. Pesko, Z. Feng, S. Sawhney, J. Newman, V. Srinivasan, and N. P. Balsara, *J. Electrochem. Soc.*, **165**, A3186 (2018).
30. Y. Lee, B. Ma, and P. Bai, *Mater. Today Energy*, **27**, 101037 (2022).
31. A. Mistry, V. Srinivasan, and H. G. Steinrück, *Adv. Energy Mater.*, **13**, 2203690 (2023).
32. A. Mistry, L. S. Grundy, D. M. Halat, J. Newman, N. P. Balsara, and V. Srinivasan, *J. Electrochem. Soc.*, **169**, 040524 (2022).
33. D. M. Halat, C. Fang, D. Hickson, A. Mistry, J. A. Reimer, N. P. Balsara, and R. Wang, *Phys. Rev. Lett.*, **128**, 198002 (2022).
34. J. Newman, J. Bennion, and C. Tobias, *Berichte der Bunsengesellschaft für Phys. Chemie*, **69**, 608 (1965).
35. K. W. Gao and N. P. Balsara, *Solid State Ionics*, **364**, 115609 (2021).
36. P. Bai, J. Li, F. R. Brushett, and M. Z. Bazant, *Energy Environ. Sci.*, **9**, 3221 (2016).
37. K. H. Chen, K. N. Wood, E. Kazyak, W. S. Lepage, A. L. Davis, A. J. Sanchez, and N. P. Dasgupta, *J. Mater. Chem. A*, **5**, 11671 (2017).
38. C. Monroe and J. Newman, *J. Electrochem. Soc.*, **150**, A1377 (2003).
39. D. Lu et al., *Adv. Energy Mater.*, **5**, 1 (2015).
40. G. Bieker, M. Winter, and P. Bieker, *Phys. Chem. Chem. Phys.*, **17**, 8670 (2015).
41. Z. J. Hoffman, A. S. Ho, S. Chakraborty, and N. P. Balsara, *J. Electrochem. Soc.*, **169**, 043502 (2022).
42. D. B. Shah, H. K. Kim, H. Q. Nguyen, V. Srinivasan, and N. P. Balsara, *J. Phys. Chem. C* (2019).